Journal of Hepatocellular Carcinoma

Dovepress
Taylor & Francis Group

Open Access Full Text Article

ORIGINAL RESEARCH

Near-Infrared Fluorescent Probes Targeting LAG-3 for Guiding Immunomodulation and Efficacy Monitoring of Stereotactic Body Radiotherapy in Liver Cancer

Qingyun Lu[1], Peng Zeng[2], Yanli An[3], Yingyu Qin[4], Jing Zhang[1], Muhao Xu[1], Cheng Wang[1], Ming Wu[1], Rong Chen[5]

[1]Department of Radiation Oncology, Medical School of Southeast University, Nanjing, Jiangsu, People's Republic of China; [2]Department of Oncology, Zhongda Hospital Affiliated to Southeast University, Nanjing, Jiangsu, People's Republic of China; [3]Department of Radiology, Medical School of Southeast University, Nanjing, Jiangsu, People's Republic of China; [4]Department of Pathogenic Biology and Immunology, Medical School of Southeast University, Nanjing, Jiangsu, People's Republic of China; [5]Department of Radiation Oncology, Zhongda Hospital Affiliated to Southeast University, Nanjing, Jiangsu, People's Republic of China

Correspondence: Rong Chen, Department of Radiation Oncology, Zhongda Hospital Affiliated to Southeast University, Nanjing, Jiangsu, 210009, People's Republic of China, Email 101011581@seu.edu.cn

Journal of Hepatocellular Carcinoma downloaded from https://www.dovepress.com/
For personal use only.

Purpose: Lymphocyte activation gene 3 (LAG-3) is an attractive biomarker for immunotherapy in hepatocellular carcinoma (HCC) due to its high expression. Based on our previously identified LAG-3 peptide, we developed a LAG-3 targeted peptide probe named Cqy-12-Cy5 for monitoring the dynamic regulation of LAG-3 by stereotactic body radiotherapy (SBRT), thereby providing a strategy to enhance the immunotherapeutic efficacy for HCC.

Methods: Immunohistochemistry (IHC) was used to detect the expression of LAG-3 in HCC tissues and its correlation with clinicopathological characteristics. An optical fluorescent probe (Cqy-12-Cy5) was constructed, and its in vivo targeting ability and metabolic profile were evaluated via near-infrared fluorescent (NIRF). Flow cytometry (FCM) was employed to assess the apoptosis of H22 cells after radiation, aiming to screen the optimal radiation dose. Furthermore, the regulatory effect of SBRT on LAG-3 expression in HCC was detected, along with changes in the proportion of $CD8^+$ T cells, TNF-α and IFN-γ following SBRT. Dynamic observations of tumor growth and LAG-3-targeted fluorescent expression after SBRT were performed using magnetic resonance imaging (MRI) and NIRF.

Results: LAG-3 is highly expressed in HCC and is closely related to tumor progression. The fluorescent uptake of the Cqy-12-Cy5 in the tumor region reached a peak at 1 hour after tail vein injection. A radiation dose of 6 Gy was identified as the optimal dose. SBRT could reduce the size of the tumor, promote $CD8^+$ T cell infiltration and increase the secretion of TNF-α and IFN-γ.

Conclusion: The successfully constructed LAG-3-targeting NIRF probe enables non-invasive, real-time monitoring of tumor growth and LAG-3 expression. SBRT can inhibit tumor growth, modulate LAG-3 expression, promote T cell infiltration and cytokine secretion in HCC. The Cqy-12-Cy5 can dynamically monitor the modulation of LAG-3 by SBRT, providing a strategy for guiding the timing of combination therapy and promoting synergistic immunotherapeutic efficacy.

Keywords: hepatocellular carcinoma, lymphocyte activation gene 3 (LAG-3), peptide probe, stereotactic body radiotherapy, immune modulation

Introduction

Primary hepatic carcinoma is a highly prevalent malignant tumor globally with a poor prognosis, ranking sixth in incidence and third in mortality worldwide. Hepatocellular carcinoma (HCC) accounts for approximately 75–85% of cases.[1] HCC has an insidious onset, with about 70–80% of patients diagnosed at an advanced stage,[2] leaving limited treatment options. The objective response rate (ORR) to single-agent programmed death receptor 1 (PD-1) inhibitor

https://doi.org/10.2147/JHC.S584426
Received: 30 December 2025
Accepted: 23 April 2026
Published: 17 June 2026

© 2026 Lu et al. This work is published and licensed by Dove Medical Press Limited. The full terms of this license are available at https://www.dovepress.com/terms.php and incorporate the Creative Commons Attribution – Non Commercial (unported, v4.0) License (http://creativecommons.org/licenses/by-nc/4.0/). By accessing the work you hereby accept the Terms. Non-commercial uses of the work are permitted without any further permission from Dove Medical Press Limited, provided the work is properly attributed. For permission for commercial use of this work, please see paragraphs 4.2 and 5 of our Terms (https://www.dovepress.com/terms.php).

therapy is only 20-30%.[3] Therefore, exploring new sensitive immune checkpoints and immunomodulatory strategies to further enhance the tumor immune response rate is a crucial direction for breaking through the limitations of immunotherapy efficacy in advanced HCC.

Stereotactic body radiotherapy (SBRT), as a high-precision radiotherapy technique, can effectively kill tumor cells while maximizing protection of surrounding normal tissues. It offers advantages such as high single doses, short treatment courses, definite efficacy, non-invasiveness, and mild adverse effects. SBRT has a dual role in tumor immunomodulation:[4–9] on the one hand, it can promote antigen release and presentation by inducing immunogenic cell death (ICD), activating the type I interferon signaling pathway, increasing major histocompatibility complex class-I (MHC-I) molecule expression, and releasing inflammatory factors, thereby promoting T cell proliferation and exerting anti-tumor effects. On the other hand, chronic interferon signaling stimulation can induce the expression of programmed cell death ligand 1 (PD-L1) on tumor cells and upregulate inhibitory receptors on T cells, such as PD-1 and cytotoxic T-lymphocyte-associated antigen 4 (CTLA-4), thus promoting immune escape. Current clinical methods for evaluating the efficacy of immune checkpoint molecules are invasive, suffer from spatiotemporal heterogeneity, and cannot achieve real-time, dynamic, and non-invasive monitoring. This makes it difficult to identify the optimal timing for combining SBRT with immune checkpoint inhibitors (ICIs) to fully leverage the positive immunomodulatory effects of SBRT.

Lymphocyte activation gene 3 (LAG-3), also known as CD223, is a key inhibitory immune receptor that promotes tumor immune escape by mediating T cell exhaustion.[10] HCC typically establishes a profoundly immunosuppressive tumor microenvironment, which is characterized by the functional exhaustion of $CD8^+$ cytotoxic T cells, massive infiltration of immunosuppressive cells such as regulatory T cells and myeloid-derived suppressor cells, and the disorder of pro-inflammatory and inhibitory cytokine networks. These pathological alterations severely impair anti-tumor immune surveillance and serve as the core driver of tumor immune escape and malignant progression.[10] LAG-3 is highly expressed on tumor-infiltrating lymphocytes (TILs) in various malignancies, including liver cancer, and its expression level is significantly correlated with tumor progression and poor prognosis.[11,12] Hepatitis B virus (HBV) infection is a major etiology of liver cancer in Asia. During chronic HBV infection, HBV-related lymphocytes can upregulate LAG-3 expression.[13] LAG-3 can directly inhibit T cell proliferation and activation through negative regulation or modulate immune responses via the secretion of immunosuppressive cytokines. Consequently, as a key regulatory molecule in the HCC immune microenvironment, the expression characteristics of LAG-3 can not only be used for disease assessment but also serve as an immunotherapeutic target, providing a new direction for HCC treatment.

Traditional pathological detection methods, such as immunohistochemistry (IHC) and blood tumor markers, are invasive, have temporal and spatial heterogeneity, and lack standardized criteria.[14–16] Imaging examinations can show "pseudo-progression" and also fail to provide information about the immune environment.[17,18] Therefore, there is an urgent need to develop molecular recognition and monitoring systems with high specificity, stable binding, and real-time monitoring capabilities. Compared to monoclonal antibodies and nanobodies, peptides offer advantages such as ease of synthesis, high targeting specificity, low immunogenicity, and rapid metabolic clearance.[19] Combining synthetic probes with near-infrared fluorescence (NIRF) imaging holds promise for enabling real-time monitoring of the dynamic regulation of immune checkpoints (ICs) by SBRT. For instance, an Arg-Gly-Asp (RGD) peptide conjugate coupled with the Cyanine 7 (Cy7) fluorescent dye has been successfully applied for PD-L1 imaging in liver cancer, with a targeting efficiency exceeding 90%.[20] This technology provides a powerful molecular imaging tool for intraoperative real-time navigation and dynamic assessment of therapeutic efficacy.

This study aims to investigate the expression characteristics of LAG-3 in HCC and its potential as a diagnostic and therapeutic biomarker. We plan to identify high-affinity LAG-3-targeting peptides using phage display technology and construct LAG-3-targeting peptide probes. The study will also evaluate the modulation of the HCC immune microenvironment, particularly LAG-3 expression by SBRT. By integrating advanced imaging technologies, we hope to non-invasively and in real-time detect changes in LAG-3 in HCC and the effects of SBRT on tumor growth and immune responses. This approach aims to guide the optimal timing for combining radiotherapy with immune checkpoint inhibitors, promote synergistic immunotherapeutic efficacy, and provide new insights for developing novel integrated diagnostic and therapeutic tools for HCC.

 https://doi.org/10.2147/JHC.S584426

Materials and Methods

Clinical Data

Clinical data from 40 patients with liver cancer treated at Zhongda Hospital Affiliated to Southeast University between 2018 and 2022 were selected. The collected case information included gender, age, pathological staging (according to the TNM staging principles), number of tumors, tumor diameter, vascular invasion, lymph-node metastasis, and distant metastasis. The specimens included both hepatocellular tumor tissues (T) and adjacent non-tumor tissues (N). All patients were confirmed to have liver cancer by pathological biopsy. The tissue sections were embedded in paraffin, dewaxed, hydrated, antigen-repaired, incubated with antibodies, stained, and mounted, and finally quantitatively analyzed using the H-score method. This study has been approved by the Ethics Review Committee of Zhongda Hospital affiliated to Southeast University (2021ZDSYLL219-P01).

Cell Culture and Animal Model Construction

The mouse hepatoma cell line H22 was purchased from the Chinese Academy of Sciences Committee on Type Culture Collection (Catalog No: SCSP: 478). H22 cells were cultured in Roswell Park Memorial Institute 1640 medium (RPMI 1640, Corning, USA) containing 10% fetal bovine serum (FBS, Gibco, USA) and 10% penicillin/streptomycin (P/S, Gibco, USA) in a humidified environment with 5% CO_2 at 37°C. All animal experiments were approved by the Animal Ethics Committee of Southeast University and conducted in accordance with the Regulations for the Administration of Laboratory Animals in China. Laboratory animal license No: SYXK (Su) 2021–0021. Six-week-old male BALB/c mice (Vital River Laboratory Animal Technology, China) were housed in the animal center of Southeast University's laboratory. Subcutaneous tumor models in mice were constructed by injecting 1×10^6 H22 cells into the back of each mouse. When the subcutaneous tumor diameter reached 5–9 mm, fresh tumor tissue was selected, cut into approximately 1 mm^3 tumor blocks, and implanted into the left lobe of the liver under 1.5% isoflurane anesthesia delivered via a gas anesthesia machine. An ophthalmic scissors was used to create a transverse incision about 2 mm wide and 4 mm deep in the left lobe of the liver, and the pre-separated tumor block was placed into the incision using ophthalmic forceps. The incision was sealed with tissue glue and sutured layer by layer. The size of subcutaneous tumors was measured with a caliper every other day, and tumor growth was recorded. Tumor volume was calculated using the formula: $V\ (mm^3) = \text{length} \times \text{width}^2 \times 0.5$. The size of orthotopic tumors was measured every two days using a 7.0T animal magnetic resonance imaging (MRI) system (BRUKER, Germany). The subcutaneous and orthotopic tumor mouse radiotherapy models received a dose of 6 Gy, with the electron linear accelerator parameters *(RS* 2000 Pro, RADSOURCE, USA) set at 6 MV and 600 MU/min, using X-ray radiotherapy.

Recombinant LAG-3 Antigen Expression and Purification

To obtain recombinant LAG-3 protein, the LAG-3 gene (available from PubMed) was first inserted into the BamHI and EcoRI sites of the PET28-A vector (+). The recombinant plasmid was transformed into BL21 (DE3) competent Escherichia coli and cultured in Luria broth containing ampicillin at 37°C until the optical density (OD) value reached 0.6–0.8. Then, 1 μM isopropyl β-D-1-thiogalactopyranoside (IPTG) was added to induce protein expression. The bacterial culture was centrifuged at 5000 rpm for 10 minutes to collect the precipitate, which was resuspended in lysis buffer containing 8 M urea and 50 mM Tris (pH 7.4). After thorough lysis under high pressure, the lysed bacteria were centrifuged at 15000 rpm for 30 minutes and loaded onto a nickel resin binding (column affinity chromatography) column. The recombinant LAG-3 protein was eluted with a high-intensity buffer containing 300 mM imidazole and verified by 10% SDS-PAGE and Coomassie Blue staining, yielding the purified recombinant LAG-3 protein.

Construction of LAG-3-Targeted Peptide Probes

The purified LAG-3 protein was coated on a 96-well plate, and phage display technology was used for screening. 50 μL of phage supernatant was added to the 96-well plate coated with LAG-3 protein for screening. Unbound phages were eluted with 0.2 M pH 2.2 Gly-HCl, followed by neutralization with 1 M pH 9.1 Tris-HCl. The bound phages were collected, diluted by factors of 1000, 10000, etc, and transferred into E. coli for amplification. The above screening method was repeated three times to obtain the desired high-affinity clones. The clones were sequenced to obtain the target amino acid sequence in reverse. The sequence with the highest affinity and frequency was chemically synthesized and conjugated with a Cy5 fluorescent group to form the LAG-3-targeted peptide probe. All peptides were chemically synthesized by solid-phase Fmoc method and purified by high-performance liquid chromatography (HPLC) and electrospray ionization mass spectrometry, with a minimum purity of 95%.

Flow Cytometry (FCM)

H22 cells were cultured in culture flasks and divided into Ctrl, 4 Gy, 6 Gy, and 8 Gy groups. The electron linear accelerator parameters were set at 6 MV and 600 mu/min, and X-ray radiotherapy was applied according to the different group doses. After 24 hours of continued culture in the incubator, the cells were centrifuged, gently washed 2–3 times with pre-cooled phosphate buffered saline (PBS, Gibco, USA), and resuspended in an appropriate amount of PBS to a concentration of about 1×10^6 cells/mL. 100 μL of cell suspension was taken, mixed with 5 μL of Annexin V-FITC staining solution (Simu Biotechnology, China), and incubated in the dark at room temperature for 10 minutes. 5 μL of PI staining solution (Simu Biotechnology, China) was added, mixed, and incubated in the dark at room temperature for another 5 minutes. After adding 400 μL of pre-cooled PBS and mixing, the cells were analyzed by FCM (BD Biosciences, USA). The results were analyzed three times using FlowJo software (v7.6, OR, USA).

Immunoregulation by Flow Cytometry (IR-FCM)

After the mice were euthanized by cervical dislocation, the tumor tissues were removed and placed in serum-free RPMI 1640 culture medium. The tumor tissues were minced with ophthalmic scissors and transferred to a cell culture incubator for digestion for 1 hour in tissue digestion solution (0.5 mg/mL hyaluronidase (Labgic Technology, China) + 0.2 mg/mL collagenase V (Labgic Technology, China)). The digested tumor was placed on a 70 μm cell strainer and ground with a pestle. The homogenate was filtered through a 70 μm filter, and the cell suspension was collected. The cells were centrifuged, resuspended in 2 mL 1x Lysing solution (Labgic Technology, China), and incubated in the dark to lyse red blood cells. After another centrifugation, the cells were resuspended in 1 mL Dulbecco's phosphate buffered saline (DPBS, Gibco, USA). Anti-LAG-3 primary antibody (Cell Signaling Technology, USA), goat anti-rabbit secondary antibody (Santa Cruz, USA), CD45 antibody (Thermo Fisher Scientific, USA), CD3 antibody (Thermo Fisher Scientific, USA), CD8 antibody (Thermo Fisher Scientific, USA), TNF-α antibody (Thermo Fisher Scientific, USA), and IFN-γ antibody (Thermo Fisher Scientific, USA) were added. After incubation in the dark, the cells were washed three times with PBS and analyzed by FCM for fluorescence. The live cell count for each sample was 1×10^6. The results were analyzed three times using FlowJo software.

Near-Infrared Fluorescence Imaging

Subcutaneous tumor-bearing mice were divided into two groups and injected intravenously with 20 mg of Ctl-Cy5-peptide or Cqy-12-Cy5-peptide. Under anesthesia with isoflurane and oxygen, in vivo fluorescence imaging was performed at different time points (0.5, 0.75, 1, 2, 4, 8 h) after injection using the IVIS-Spectrum system (Perkin Elmer, Santa Clara, CA, USA). The excitation and emission wavelengths of the probe were 620 nm and 670 nm, respectively. After the mice were euthanized by cervical dislocation, the tumors and major organs were dissected for ex vivo near-infrared imaging. The above steps were repeated three times to determine the imaging characteristics and metabolic patterns of the LAG-3 probe. For orthotopic tumor-bearing mice, the liver was exposed along the midline under anesthesia with isoflurane and oxygen, and 20 mg of Cqy-12-Cy5-peptide was injected intravenously. In vivo fluorescence imaging was performed 1 hour after injection using the IVIS-Spectrum system. After the mice were euthanized by cervical dislocation, the tumors and major organs were dissected for ex vivo near-infrared imaging.

Bioluminescence Imaging

Subcutaneous tumor-bearing mice were divided into two groups and injected intraperitoneally with d-luciferin potassium salt. Under anesthesia with isoflurane and oxygen, bioluminescence imaging was performed at the same time point after injection using the IVIS-Spectrum system (Perkin Elmer, Santa Clara, CA, USA). Imaging was performed one day before the first radiotherapy, one day after the first radiotherapy, and one day after the last radiotherapy.

Statistical Analysis

Comparisons between groups were made using the two-independent-sample *t*-test or one-way analysis of variance. The significance threshold was set at $P < 0.05$ (*$P < 0.05$, **$P < 0.01$, ***$P < 0.001$, ****$P < 0.0001$). Statistical analysis was performed using GraphPad Prism software (V9.0, CA, USA).

Results

Relationship Between LAG-3 and Clinical Characteristics of HCC

Using immunohistochemistry, we detected the expression of LAG-3 protein in human hepatocellular carcinoma tumor tissues and adjacent non-tumor tissues. Among the paraffin sections of 40 cases of tumor tissues and adjacent non-tumor tissues (Figure 1A), the expression level of LAG-3 in liver tumor tissues was significantly higher than that in adjacent non-tumor tissues (Figure 1B, 1E and Table 1, $P < 0.001$). Additionally, we found that the expression level of LAG-3 protein was higher in intermediate and advanced stages than in early-stages (Figure 1C, 1E and Table 1, $P < 0.001$), and higher in HCC tumor tissues with distant metastasis than in those without (Figure 1D, 1G and Table 1, $P = 0.051$). Therefore, LAG-3 is positively correlated with the malignant progression of HCC and is not statistically different from gender, age, tumor number, tumor diameter, vascular invasion or lymph node metastasis (Table 1, $P > 0.05$).

Construction of LAG-3-Targeted Peptide Probes and in vivo Uptake Rate

The LAG-3 gene was cloned into the pET28a(+) vector and transformed into BL21 (DE3) E. coli. After induction with IPTG, the target protein was purified by nickel affinity chromatography. The purity was approximately 85% with a relative molecular weight of 51 kDa as detected by SDS-PAGE (Figure 2B). A phage display library was successfully constructed and amplified in E. coli. The phages from the library were incubated with LAG-3 protein for specific binding. After washing and amplification in E. coli, 13 sequences with strong binding ability to the target protein were successfully selected. Among them, the sequence SAMTPQKYWYRT had the highest optical density (OD) value at 450 nm (4.2027) and was selected as the target sequence, named Cqy-12. After adding a Cy5 fluorescent label, the probe was successfully prepared and named Cqy-12-Cy5. The protein from the negative control group was combined with Cy5 to prepare the blank control probe, named Ctl-Cy5 (Figure 2A and C). To explore the in vivo absorption time and metabolic behavior of the probe, we established a subcutaneous HCC mouse model. The Cqy-12-Cy5 and Ctl-Cy5 probes were injected intravenously into the mice, and near-infrared fluorescence in vivo imaging was performed at six time points (0.5 h, 0.75 h, 1 h, 2 h, 4 h, and 8 h) after injection. The results showed that the fluorescence intensity (FI) in the subcutaneous HCC gradually increased over time, reaching a peak at 1 h after injection. Thereafter, the FI value began to decline. The FI values of the Cqy-12-Cy5 group were significantly higher than those of the Ctl-Cy5 group (Figure 2D and E, $P < 0.0001$). This indicates that 1 h is the optimal time for in vivo imaging after probe injection. At 1 h, the subcutaneous tumor mouse model was dissected, and the tumor and major organs were imaged ex vivo. The image and statistical results showed that the Cqy-12-Cy5 probe was mainly metabolized by the liver and kidneys (Figure 2F and G).

Effect of Radiotherapy on the Biological Activity of HCC

H22 cells were irradiated with 0, 4 Gy, 6 Gy, and 8 Gy of radiation. After 72 hours of culture, cell apoptosis rates were detected by FCM. The results showed that the apoptosis rate of H22 cells increased continuously with the increase of radiation dose, reaching a peak at 6 Gy (Figure 3A and B, $P < 0.05$). The total apoptosis rate of H22 cells was highest at 6 Gy. The apoptosis rate decreased at 8 Gy. Therefore, 6 Gy was selected as the optimal dose for inducing cell apoptosis. We also constructed a subcutaneous HCC mouse model and irradiated it with 0, 4 Gy, 6 Gy, and 8 Gy of SBRT. The expression of LAG-3 in lymphocytes in the tumor tissues of mice after SBRT was detected by FCM. The results showed

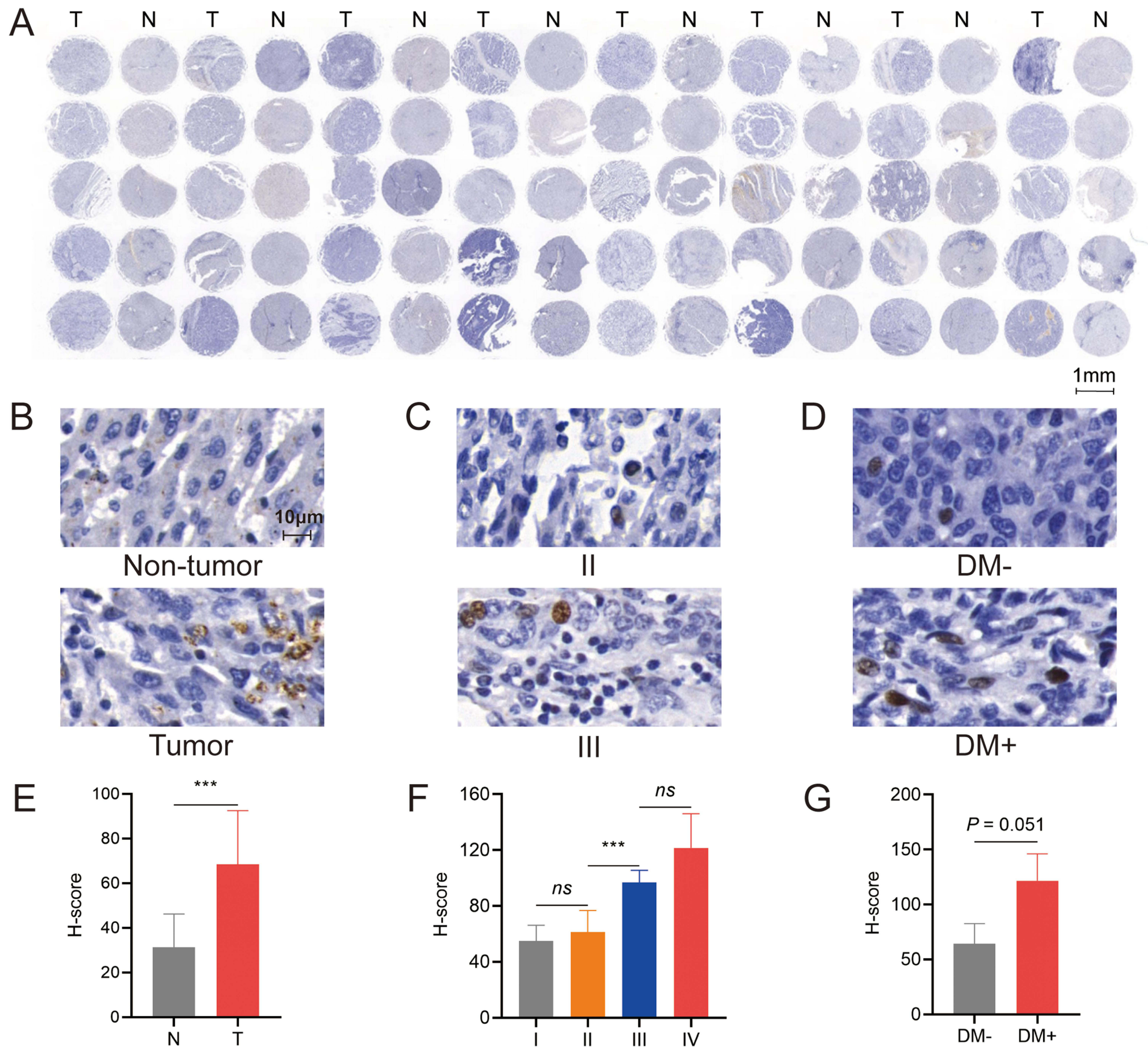

Figure 1 The relationship between LAG-3 and clinical characteristics of HCC samples. (**A**) The expression of LAG-3 protein in human hepatocellular carcinoma tumor tissues and adjacent non-tumor tissues detected by immunohistochemistry. (**B**) Representative LAG-3 staining of tumor tissues and adjacent non-tumor tissues. (**C**) Representative LAG-3 staining of stage II and stage III. (**D**) Representative LAG-3 staining of tumor tissues with or without distant metastasis. (**E**) The comparison of H-scores between tumor tissues and adjacent non-tumor tissues. (**F**) The comparison of H-scores between stage II and stage III. (**G**) The comparison of H-scores between tumor tissues with or without distant metastasis. A scale bar: 1mm. B-D scale bar: 10 μm. ***P < 0.001.

Abbreviations: N, non-tumor tissue; T, tumor tissue; II, stage II; III, stage III; DM-, without distant metastasis; DM+, with distant metastasis; H-score, histochemistry score; ns, no statistical difference.

that the LAG-3 fluorescence value was lowest at 6 Gy (Figure 3C and D, $P < 0.01$). Therefore, we chose 6 Gy for subsequent experiments.

SBRT Promotes $CD8^+$ T Cell Infiltration in HCC

To explore the immune regulatory effects of SBRT on HCC, we constructed a subcutaneous HCC mouse model and irradiated it with the optimal radiation dose (6 Gy) selected earlier. In vivo imaging was performed on the mice in each group, and the growth of subcutaneous tumors was monitored. The results showed that the average bioluminescence intensity of the tumors in the irradiated group was lower than that in the tumor control group (Figure 4A and B, $P < 0.0001$). The tumor volume in the irradiated group was also significantly smaller than that in the tumor control group

 https://doi.org/10.2147/JHC.S584426

Table 1 The Relationship Between LAG-3 and Clinical Characteristics of HCC Cases

Characteristics	Classification	Cases	H-score: mean ± SD	P-value
Tissue	Non-tumor tissue	40	68.55±23.98	<0.001
	Tumor tissue	40	31.29±14.88	
Gender	Male	37	67.42±24.50	0.087
	Female	3	82.43±9.69	
Age	<65	31	66.91±24.84	0.394
	≥65	9	74.20±21.01	
TNM stage	I	5	54.94±11.30	<0.001
	II	28	61.26±15.43	
	III	4	96.88±8.67	
	IV	3	121.51±24.62	
Number of tumor	1	30	64.32±20.15	0.458
	>1	10	72.15±26.83	
Diameter of tumor (cm)	<5	12	67.52±23.16	0.876
	≥5	28	65.87±22.49	
Vasculature infiltration	Yes	16	66.69±26.47	0.704
	No	24	69.79±22.66	
Lymph-node metastasis	Yes	2	118.00±33.74	0.268
	No	38	65.95±20.88	
Distant metastasis	Yes	3	121.51±24.62	0.051
	No	37	64.25±18.34	

Abbreviations: H-score, histochemistry score; SD, standard deviation.

(Figure 4A and C, P < 0.0001). On this basis, lymphocytes were separated from the tumor tissues of mice, and the proportion of $CD8^+$ T cells was detected by FCM. The proportion of $CD8^+$ T cells in the irradiated group was higher than that in the normal mouse group and the tumor control group (Figure 4D, P < 0.0001). The proportion of TNF-α and IFN-γ secreted by $CD8^+$ T cells in the irradiated group was also higher than that in the normal mouse group and the tumor control group (Figure 4E and F, P < 0.0001). Therefore, we believe that SBRT can promote the infiltration of $CD8^+$ T cells and activate T cell immunity.

Monitoring of LAG-3 Uptake and Expression in Subcutaneous HCC After SBRT by Probe

Based on the optimal radiation dose of 6 Gy, we constructed a subcutaneous HCC mouse model and injected the Cqy-12-Cy5 probe intravenously into the mice. Near-infrared fluorescence in vivo imaging was performed 1 h after injection. The results showed that the FI value in the irradiated group was significantly lower than that in the tumor control group (Figure 5A and B, P < 0.001). The ex vivo imaging of the tumor and major organs at 1 h showed that the FI value of the tumor in the irradiated group was lower than that in the tumor control group, while there was no significant statistical difference in the FI values of the major organs such as the liver, kidneys, and lungs between the two groups (Figure 5C and D, P < 0.0001).

Monitoring of LAG-3 Uptake and Expression in Orthotopic HCC After SBRT by Probe

To explore the effect of SBRT on the growth of orthotopic HCC, we constructed an orthotopic HCC mouse model based on the optimal radiation dose of 6 Gy. The size of the orthotopic liver cancer in each group of mice was monitored and recorded by 7.0T magnetic resonance imaging. The results showed that the tumor volume in the irradiated group was significantly smaller than that in the tumor control group (Figure 6A and C, P < 0.0001). To explore the effect of SBRT on LAG-3 expression in orthotopic HCC, the Cqy-12-Cy5 probe was injected intravenously into the mice with orthotopic HCC. Near-infrared fluorescence in vivo imaging was performed 1 h after injection. The results showed that the FI value

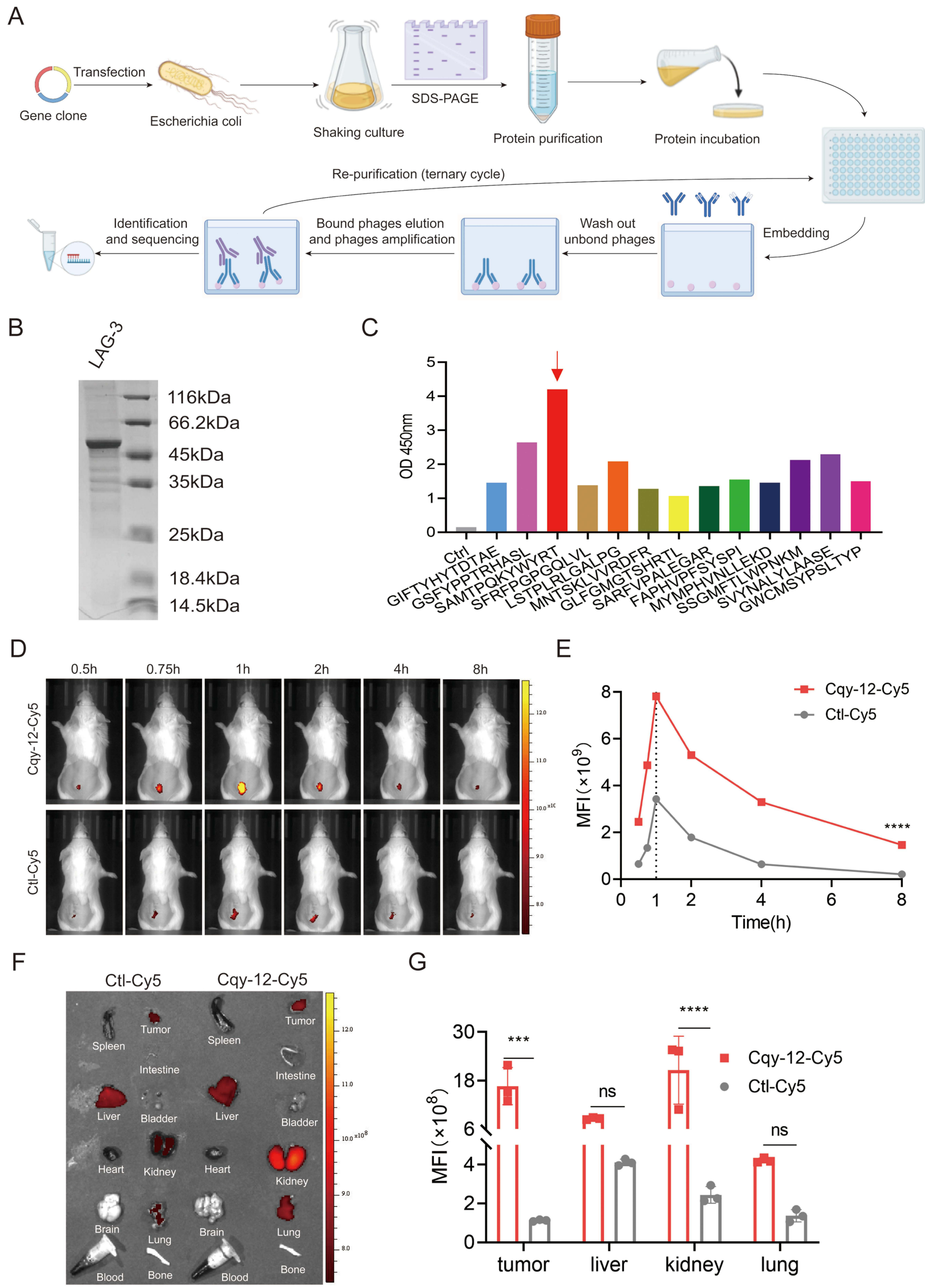

Figure 2 Screening of LAG-3-targeted peptide and near-infrared imaging of its probe. (**A**) The flow chart of the synthesis of LAG-3-targeted peptide. (**B**) Coomassie Brilliant Blue staining of LAG-3 protein after purification. (**C**) The binding affinities of selected peptide with OD value of 450nm, and the sequence names of each peptide. The red arrow indicates the target peptide. (**D**) Representative NIRF images of H22 tumor-bearing mice (n=3), after injection (i.v.) of Cqy-12-Cy5 or Ctl-Cy5, respectively. (**E**) The mean fluorescence intensity (MFI) of Cqy-12-Cy5 and Ctl-Cy5. (**F**) NIRF images of tumors and major organs (n=3) 1 h post injection (i.v.) of Cqy-12-Cy5 and Ctl-Cy5. (**G**) Biodistribution of Cqy-12-Cy5 and Ctl-Cy5. ***P < 0.001, ****P < 0.0001.

Abbreviation: ns, no statistical difference.

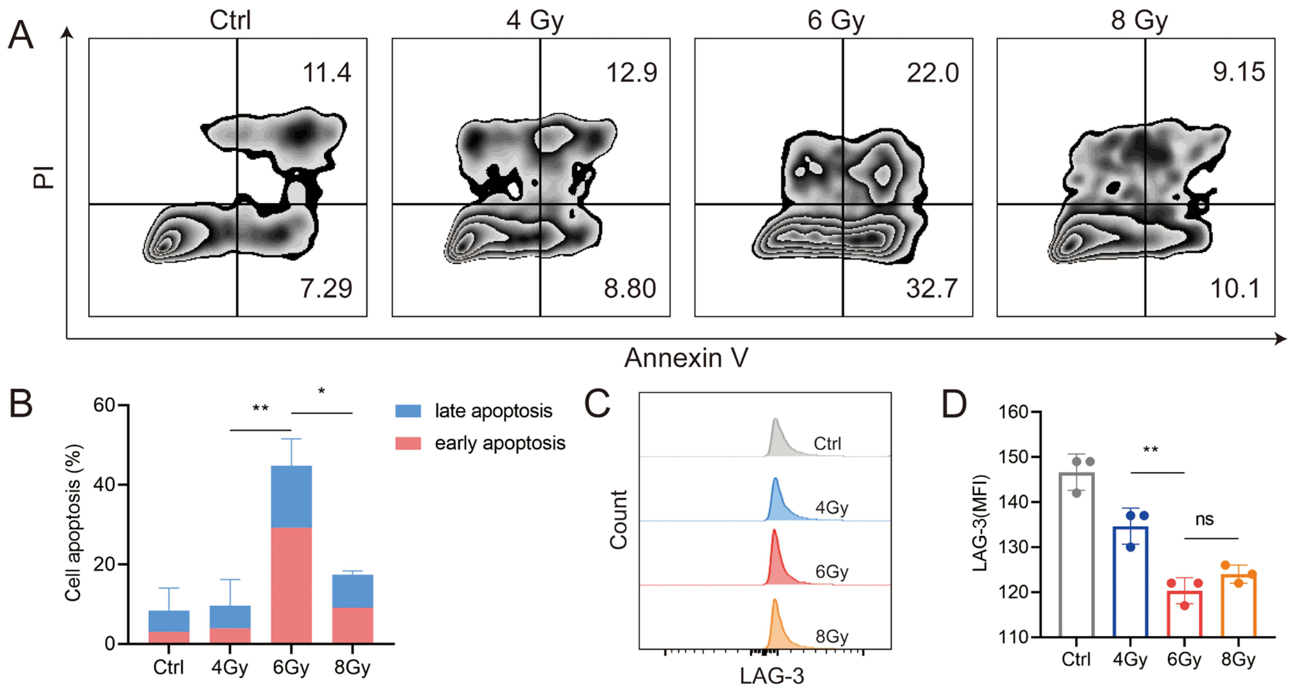

Figure 3 The effect of the biological activity of radiation in HCC. (**A**) In vitro apoptosis of H22 cells after different radiation doses by FCM (n=3). (**B**) Quantity of cell apoptosis of H22 cells after different radiation doses. (**C**) LAG-3 expression in tumor tissues after different radiotherapy doses by FCM (n=3). (**D**) The mean fluorescence intensity (MFI) of LAG-3 in tumor tissues after different radiotherapy doses. *P < 0.05, **P < 0.01.
Abbreviation: ns no statistical difference.

of the orthotopic tumor in the irradiated group was significantly lower than that in the tumor control group (Figure 6B and D, P < 0.0001). The ex vivo imaging of the tumor and major organs at 1 h showed that the FI value of the tumor in the irradiated group was lower than that in the tumor control group (Figure 6E and F, P < 0.0001).

Conclusion and Discussion

HCC is one of the most common malignant tumors of the digestive system, characterized by insidious onset, strong invasiveness, high recurrence, high metastasis rates, and extremely poor prognosis.[21,22] Globally, its morbidity and mortality have long ranked among the highest of all malignant tumors.[1] At this stage, surgical resection, interventional therapy, and radiotherapy constitute the core system of comprehensive treatment for liver cancer.[22] Among them, SBRT with its technical advantages of high precision, high dose delivery, and minimal damage to normal tissues, has become one of the first-line local treatment options for unresectable HCC.[23] Tumorigenesis and progression are not merely malignant proliferation of tumor cells, but a consequence of the interaction and dynamic imbalance between tumor cells and the immune microenvironment. Immune escape has been confirmed to be closely associated with the invasive and metastatic potential as well as the clinical prognosis of HCC.[24] LAG-3, a novel immune checkpoint molecule with the most promising clinical translational potential following PD-1, mediates the formation of an immunosuppressive tumor microenvironment by specifically binding to MHC-II and inhibiting the activation and proliferation of $CD8^+$ T cells.[10] In recent years, the rapid development of multimodal molecular imaging technology has provided a new direction for the non-invasive diagnosis and efficacy monitoring of HCC. NIFR targeted imaging, featuring high specificity, high signal-to-noise ratio, and real-time dynamic monitoring, compensates for the deficiencies of traditional imaging in the detection of tiny lesions and molecular-level efficacy evaluation.[25] Based on clinical tissue specimens, liver cancer cell models, and subcutaneous and orthotopic tumor models, this study integrated techniques including IHC, FCM, NIFR imaging, and MRI to systematically analyze the clinical expression characteristics of LAG-3 in HCC, verify the regulatory effects of SBRT on HCC cell apoptosis, LAG-3 expression, and the anti-tumor immune microenvironment, and optimize the in vivo imaging parameters of targeted fluorescent probes. This research aims to improve the theoretical system of

https://doi.org/10.2147/JHC.S584426

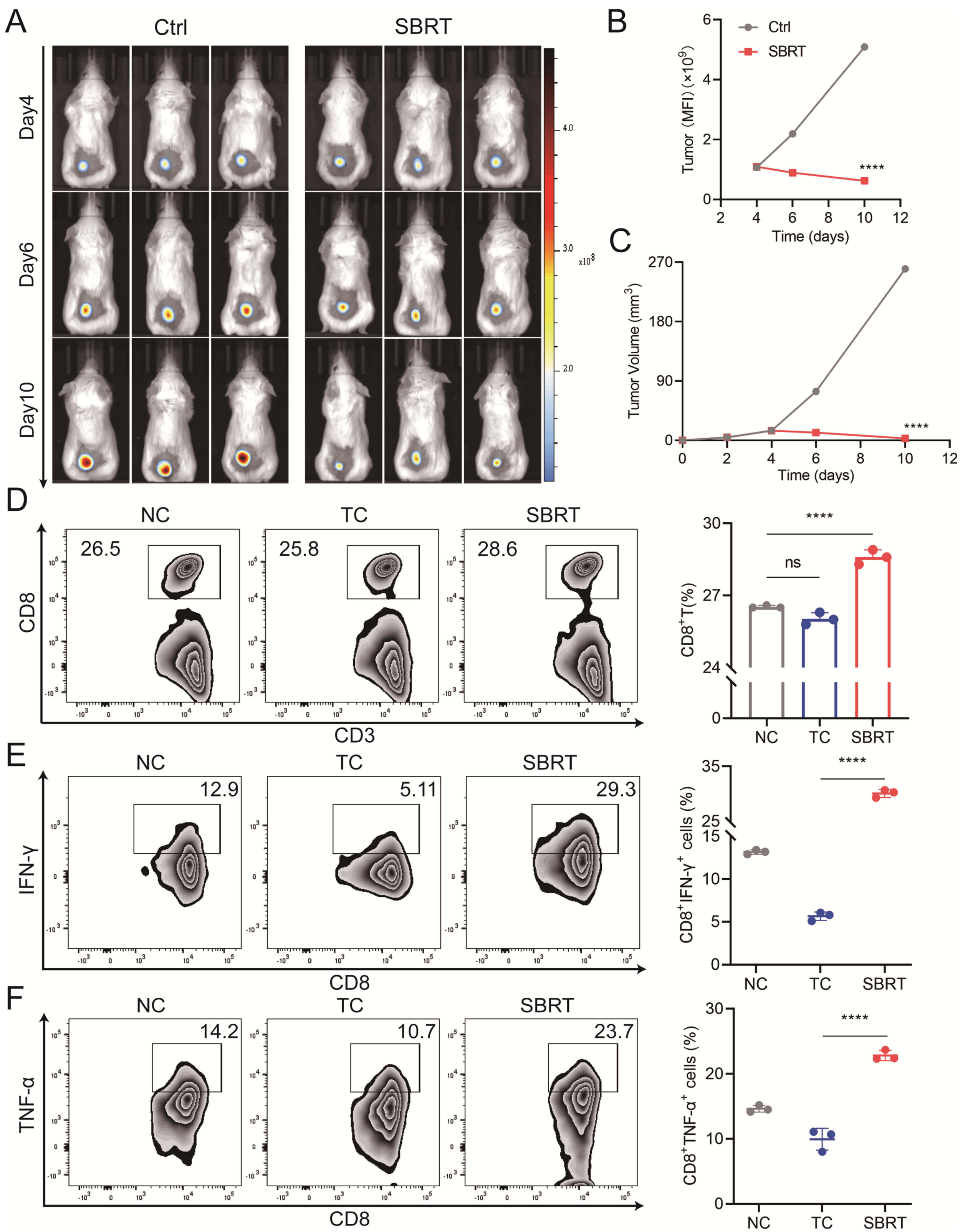

Figure 4 The infiltration of CD8$^+$ T cells in different groups after SBRT. (**A**) Representative bioluminescence imaging images of H22 subcutaneous tumor-bearing mice (n=3). (**B**) The mean fluorescence intensity (MFI) of subcutaneous tumors after SBRT. (**C**) Subcutaneous tumor volumes in different groups. (**D**) The proportion of CD8$^+$ T cell in different groups by FCM (n=3). (**E**) The proportion of IFN-γ secretion by CD8$^+$ T cells in different groups by FCM (n=3). (**F**) The proportion of TNF-α secretion by CD8$^+$ T cells in different groups by FCM (n=3). ****$P < 0.0001$.

Abbreviations: NC, normal control group; TC/Ctrl, tumor control group; SBRT, SBRT group; ns, no, statistical difference.

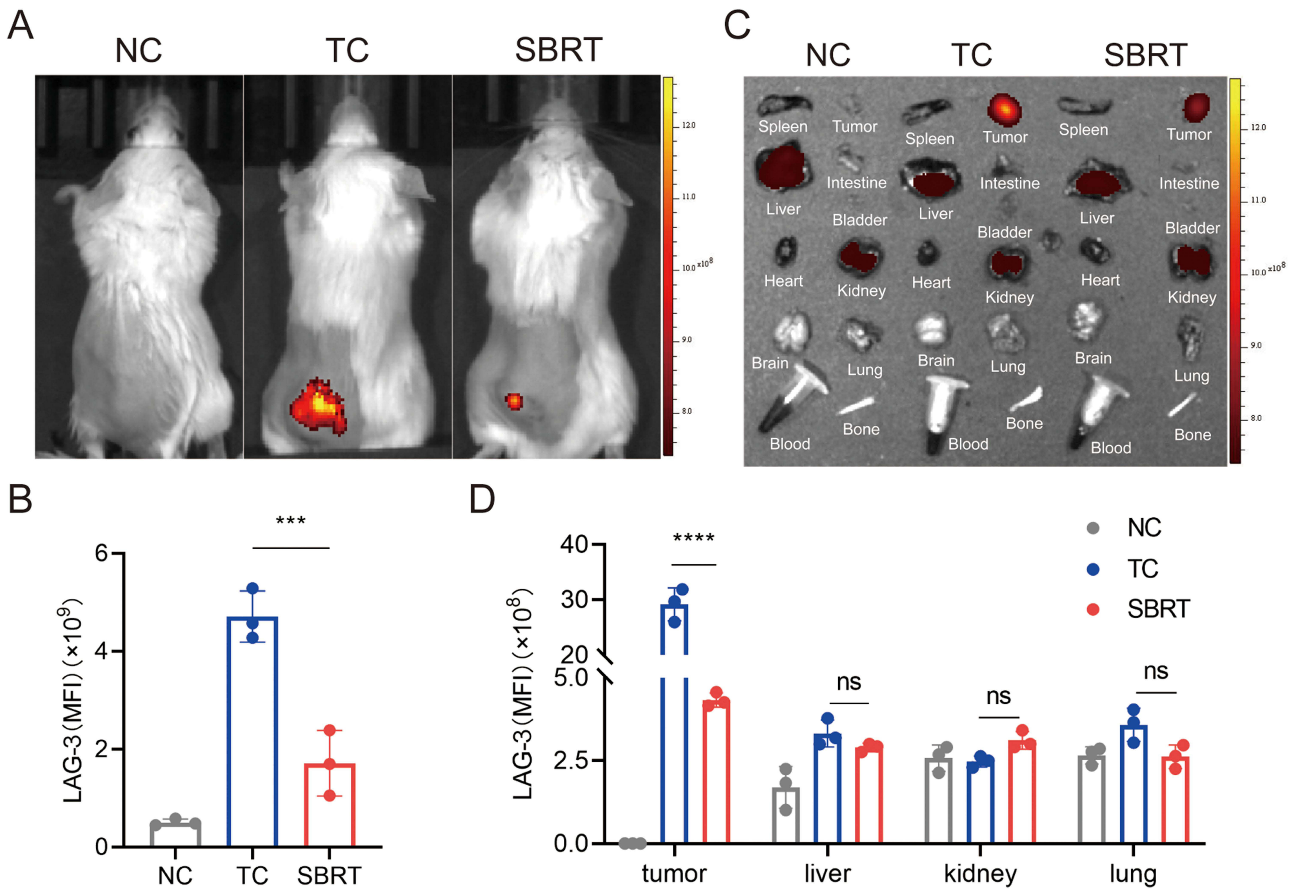

Figure 5 The expression of LAG-3 in subcutaneous tumors in mice after SBRT. (**A**) Representative NIRF images of tumors (n=3) 1 h post injection (i.v.) of Cqy-12-Cy5. (**B**) The mean fluorescence intensity (MFI) of tumors. (**C**) NIRF images of tumors and major organs (n=3). (**D**) The mean fluorescence intensity of tumors and major organs. ***$P < 0.001$, ****$P < 0.0001$.

Abbreviations: NC, normal control group; TC, tumor control group; SBRT, SBRT group; ns, no statistical difference.

radiotherapy-mediated immune regulation in HCC, and provide experimental evidence for the clinical translation of SBRT combined with LAG-3 targeted therapy as well as the multimodal imaging diagnosis and treatment of HCC.

IHC results indicated that the expression level of LAG-3 in HCC tumor tissues was significantly higher than that in paired adjacent non-tumor tissues, and was positively correlated with the clinical stage of tumors. LAG-3 expression was markedly upregulated in tumor tissues with distant metastasis compared with those without metastasis. This expression pattern is highly consistent with the distribution rule of immune checkpoint molecules in solid tumors, and is also validated by the conclusions of multiple domestic and international clinical studies on HCC. Clinical studies have revealed that LAG-3 is specifically and highly expressed in tumor tissues, and its high expression level is closely associated with tumor stage, lymph node metastasis, distant metastasis, and poor overall survival, identifying it as an independent prognostic biomarker for evaluating the malignant biological behavior of tumors.[12,26] From the perspective of molecular mechanisms, LAG-3 overexpressed in the HCC microenvironment is mainly distributed on the surface of tumor-infiltrating lymphocytes. It blocks the T cell receptor signaling pathway, inhibits the cytotoxicity of effector T cells, and simultaneously promotes the differentiation and enrichment of regulatory T cells, further exacerbating the immunosuppressive state and providing a favorable microenvironment for the proliferation, invasion, and distant metastasis of tumor cells.[27] Previous basic studies have confirmed that silencing LAG-3 expression can effectively restore the killing function of $CD8^+$ T cells and inhibit the migration and invasion of HCC cells, which inversely corroborates the correlation between high LAG-3 expression and the malignant progression of HCC observed in this study.[28] Collectively, the abnormal expression of LAG-3 is involved in the tumorigenesis, progression, and metastasis of HCC, and has clinical value as a molecular biomarker for clinical stratification and prognostic evaluation of HCC.

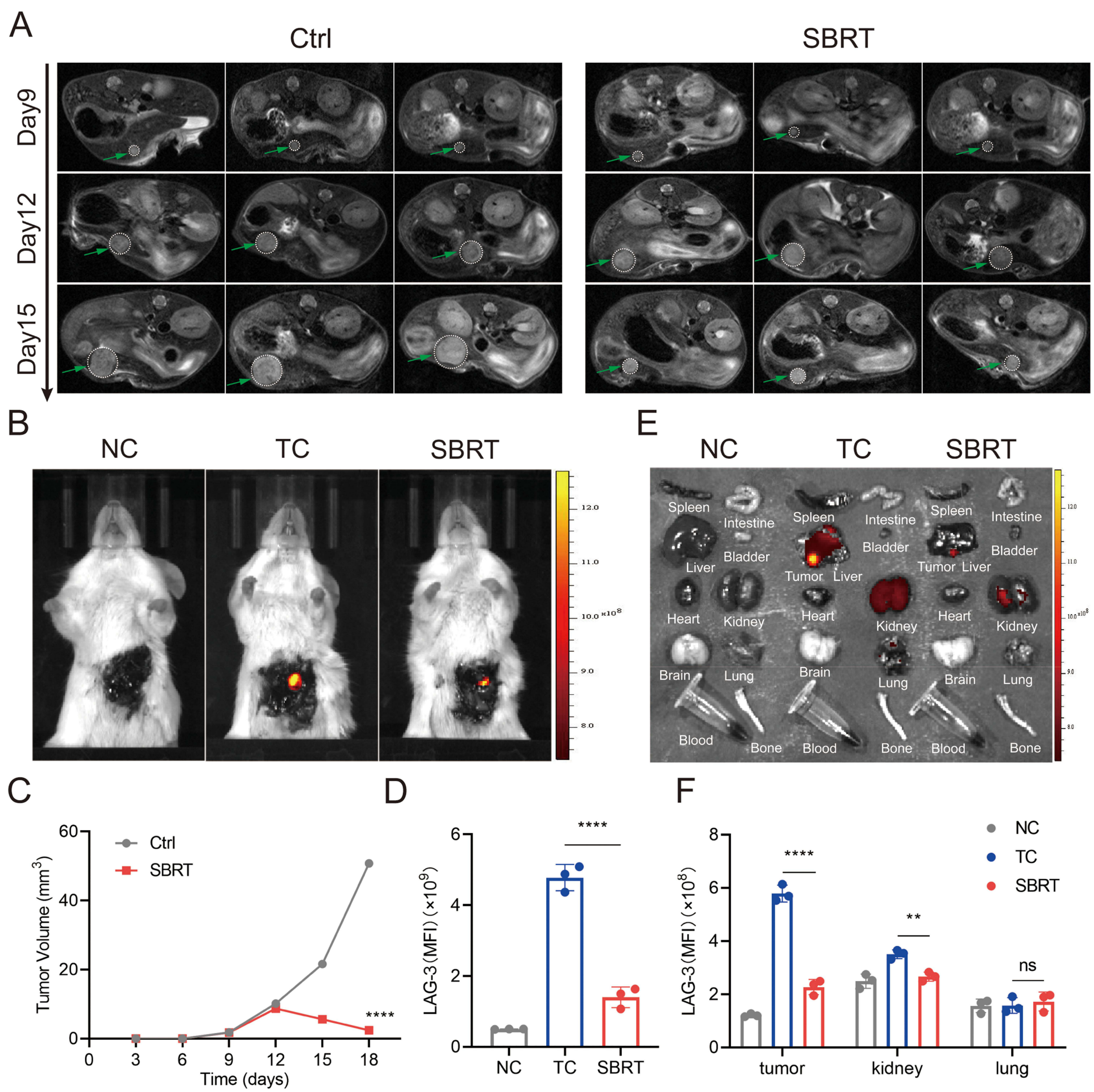

Figure 6 The expression of LAG-3 in orthotopic tumors in mice after SBRT. (**A**) Magnetic resonance imaging (n=3) and (**C**) orthotopic tumor volumes after SBRT. The green arrow indicates the tumor. (**B**) Representative NIRF images of tumors 1 h post injection (i.v.) of Cqy-12-Cy5 (n=3). (**D**) The mean fluorescence intensity (MFI) of tumors. (**E**) NIRF images of tumors and major organs (n=3). (**F**) The mean fluorescence intensity of tumors and major organs. **P < 0.01, ****P < 0.0001.
Abbreviations: NC, normal control group; TC/Ctrl, tumor control group; SBRT, SBRT group; ns, no statistical difference.

Targeted molecular imaging serves as a crucial bridge connecting basic research and clinical diagnosis and treatment. The LAG-3 targeted peptide probe constructed in this study exhibited favorable tumor targeting in mouse HCC models after tail vein injection, with the fluorescence uptake in tumor regions reaching a peak at 1 hour post-injection. Quantitative analysis between groups showed an extremely statistically significant difference in fluorescence intensity. A research consensus in the field of molecular imaging holds that the in vivo pharmacokinetic characteristics of targeted probes are the core factor determining imaging quality, and the selection of the optimal imaging time window requires a balance between two key elements: specific tumor enrichment of the probe and clearance of background signals from normal tissues.[29,30] Small-molecule peptide probes possess inherent advantages of low molecular weight, strong tissue penetration, and rapid metabolic rate.[19] Their in vivo distribution relies on the dual effects of passive and active targeting: they are rapidly distributed throughout systemic tissues via blood circulation in the early stage, then achieve local enrichment through specific binding to targets on the tumor surface. After reaching the peak fluorescence signal, they are rapidly cleared through the body's metabolic pathways, with background signals gradually decreasing. In relevant studies on NIFR imaging of HCC, the optimal imaging time window for most targeted probes is concentrated at 0.5 to 2 hours after injection, and the 1 hour imaging time point determined in this study is highly consistent with research data in this field.[31] At this time point, the probe enrichment in tumor tissues is the highest and the background interference from normal tissues is the lowest, enabling high-contrast imaging of tumors and normal tissues. Meanwhile, the in vivo distribution characteristic that the probe is mainly metabolized by the liver and kidneys conforms to the classic metabolic pathway of small-molecule fluorescent probes, and also indicates that the probe has favorable biocompatibility and in vivo safety without obvious visceral accumulation toxicity, laying an imaging foundation for subsequent clinical translation.[32]

In cell experiments, radiotherapy exhibited a clear dose-dependent biological effect. With the increase of irradiation dose, it significantly induced apoptosis of H22 hepatoma cells and downregulated LAG-3 expression, among which the 6 Gy irradiation dose achieved the most prominent pro-apoptotic effect and LAG-3 inhibition. Radiotherapy intervention also effectively promoted the infiltration of $CD8^+$ T cells and upregulated the secretion levels of anti-tumor cytokines such as TNF-α and IFN-γ. The dual anti-tumor effect of radiotherapy has become a core consensus in the field of radioimmunology. Traditionally, radiotherapy exerts a direct cytotoxic effect mainly by inducing DNA double-strand breaks and activating apoptotic signaling pathways, while modern studies have confirmed that radiotherapy at an appropriate dose can break tumor immune tolerance and achieve positive remodeling of the immune microenvironment.[33,34] In vitro studies on solid tumors have demonstrated that moderate and low-dose radiotherapy can downregulate the expression of multiple immune checkpoint molecules such as PD-1, LAG-3, and TIM-3 and relieve the immunosuppressive state, which is consistent with the finding that SBRT inhibits LAG-3 expression in this study.[35] As the optimal dose screened in this study, 6 Gy balances the dual effects of directly killing tumor cells and indirectly regulating the immune microenvironment. It avoids lymphocyte depletion and aggravated immunosuppression caused by high-dose radiotherapy, and compensates for the insufficient anti-tumor effect of low-dose radiotherapy, providing accurate experimental data for the individualized optimization of SBRT dose regimens for clinical HCC. $CD8^+$ T cells are the core effector cells mediating specific anti-tumor immunity, while TNF-α and IFN-γ, as type I inflammatory cytokines, exert anti-tumor effects by enhancing T cell killing activity, inhibiting tumor angiogenesis, and inducing tumor cell apoptosis. A number of preclinical studies have shown that the immune activation effect mediated by radiotherapy is mainly dependent on the infiltration and activation of $CD8^+$ T cells, and the increased secretion of cytokines is a direct manifestation of immune microenvironment remodeling. The results of this study further improve the mechanism of SBRT regulating the immune microenvironment of HCC.[36]

The validation results of small animal in vivo models further consolidated the conclusions of in vitro experiments. In H22 subcutaneous and orthotopic HCC models, SBRT intervention significantly reduced tumor volume and markedly decreased the targeted fluorescence signal intensity in tumor regions, with MRI and NIFR imaging results providing complementary verification. Compared with subcutaneous tumor models, orthotopic HCC models can simulate the anatomical structure, blood supply characteristics, and immune microenvironment of human HCC, and thus their research results have higher clinical extrapolation value. In preclinical studies on HCC radiotherapy, a large number of animal experiments have confirmed that SBRT can significantly inhibit the growth of orthotopic HCC and prolong the survival of model animals, and the synergistic anti-tumor effect of radiotherapy combined with immune targeted therapy is significantly superior to that of monotherapy.[37,38] The reduced tumor fluorescence signal in this study not only intuitively reflects the anti-tumor effect of SBRT, but also confirms that NIFR imaging technology can be used as an effective method for non-invasive dynamic monitoring of radiotherapy efficacy, realizing the whole-process evaluation from morphological changes to molecular-level alterations and providing technical support for the improvement of the HCC efficacy evaluation system.

This study has remarkable advantages and innovations in experimental design, techniques, and research conclusions. A three-dimensional full-chain research system of "clinical tissues - cells - animal models" was constructed, and cross-

 https://doi.org/10.2147/JHC.S584426

validation was performed by integrating multiple techniques such as IHC, FCM, and multimodal imaging, which effectively avoided the limitations of a single experimental system and ensured the high reliability and stability of the research conclusions. Focusing on LAG-3, a novel immune checkpoint, this study identified 6 Gy as the optimal dose of SBRT for regulating HCC cell apoptosis and LAG-3 expression for the first time, filling the gap in the subdivision field of radiotherapy dose optimization for HCC. Meanwhile, the imaging time window of targeted fluorescent probes was optimized, and radiotherapy-mediated immune regulation was combined with molecular imaging diagnosis and treatment. The research direction conforms to the development trend of precision medicine and translational medicine, and has both theoretical innovation and clinical application value.

Limited by experimental conditions and research cycle, this study still has several limitations. In terms of clinical research, all samples were from a single center with a limited sample size and a low proportion of advanced metastatic cases, lacking validation from a multicenter large-sample cohort. Meanwhile, long-term follow-up data of patients were not included, making it impossible to clarify the quantitative correlation between LAG-3 expression and disease-free survival as well as overall survival of patients. In terms of basic mechanisms, the study only focused on phenotypic levels such as cell apoptosis, molecular expression, and immune cell infiltration, without in-depth exploration of the upstream transcriptional regulation, downstream signaling pathways, and molecular interaction networks of LAG-3 expression regulated by SBRT, resulting in insufficient depth of mechanistic research. In terms of animal experiments, no synergistic intervention study of SBRT combined with LAG-3 inhibitors was carried out, failing to quantify the synergistic mechanism and clinical benefits of the combination therapy. Additionally, there are species differences in the immune microenvironment between rodents and humans, and the clinical translation of the research results still requires further validation in large animal experiments.

The findings of this study provide multiple practical implications for the clinical diagnosis, treatment, and basic research of HCC. At the clinical application level, LAG-3 can be incorporated into the clinical pathological evaluation system of HCC as an auxiliary molecular biomarker for disease stratification, metastasis risk prediction, and radiotherapy efficacy prediction. 6 Gy can be used as the preferred intervention dose of SBRT for unresectable HCC, providing an experimental reference for the formulation of clinical radiotherapy regimens. Targeted NIFR imaging technology can be applied to the localization of tiny lesions before surgery, real-time navigation during surgery, and dynamic monitoring of efficacy after surgery for HCC, supplementing the technical shortcomings of traditional imaging. At the scientific research translation level, the mechanism by which SBRT downregulates LAG-3 expression and activates $CD8^{+}$ T cell-mediated anti-tumor immunity provides solid experimental evidence for the combination therapy strategy of SBRT plus LAG-3 targeted inhibitors. This combination regimen is expected to break through the immunosuppressive bottleneck of single radiotherapy and improve the therapeutic efficacy of advanced HCC. At the technology research and development level, the targeted fluorescent probe optimized in this study has favorable targeting and safety, providing a reference paradigm for the development and improvement of HCC-specific molecular imaging probes.

In summary, LAG-3 is abnormally and highly expressed in HCC tissues, and its expression level is closely correlated with the clinical stage and distant metastasis of tumors, making it a key molecule mediating immune escape and malignant progression of HCC. SBRT induces HCC cell apoptosis in a dose-dependent manner, downregulates LAG-3 expression, promotes $CD8^{+}$ T cell infiltration and the secretion of anti-tumor cytokines, and achieves dual anti-tumor effects of directly killing tumor cells and remodeling the immune microenvironment, with 6 Gy being the optimal intervention dose. The LAG-3 targeted NIFR probe has favorable tumor specificity and imaging efficiency, with 1 hour as the optimal imaging time window, and can be used for non-invasive diagnosis of HCC and monitoring of radiotherapy efficacy. This study systematically elucidates the clinical significance of LAG-3 in HCC and the immune regulatory mechanism of SBRT, enriches the theoretical system of radiotherapy and immunity in HCC, and provides new research ideas and experimental support for the integrated development of precision radiotherapy, immune targeted therapy, and multimodal imaging diagnosis and treatment for advanced HCC.

Statement of Ethics

This study protocol involved the use of biological specimens obtained during previous clinical diagnosis and treatment. The entire research process entailed no direct contact with or intervention in patients, and posed no adverse effects on subjects' rights or health. Based on the Institutional Review Board's assessment, the requirement for informed consent was waived, and the study was approved by the Ethics Review Committee of Zhongda Hospital affiliated to Southeast University (2021ZDSYLL219-P01). The IRB further confirmed that no information capable of identifying individual patients would be disclosed, and that the confidentiality of all data was strictly maintained throughout the study. This study was conducted in accordance with the requirements of the Declaration of Helsinki.

Funding

The authors acknowledge financial support from Jiangsu Provincial Health Commission key project (K2023005), for funding.

Disclosure

The authors report no conflicts of interest in this work.

References

1. Bray F, Laversanne M, Sung H, et al. Global cancer statistics 2022: GLOBOCAN estimates of incidence and mortality worldwide for 36 cancers in 185 countries. *CA Cancer J Clin*. 2024;74(3):229–263. doi:10.3322/caac.21834
2. Kumar K, Saraswat VA. Evolving Landscape of Systemic Therapy for Hepatocellular Carcinoma in 2025. *J Clin Exp Hepatol*. 2025;15(5):102547. doi:10.1016/j.jceh.2025.102547
3. Qin S, Chen Z, Fang W, et al. Pembrolizumab versus placebo as second-line therapy in patients from Asia with advanced hepatocellular carcinoma: a randomized, double-blind, phase III trial. *J Clin Oncol*. 2023;41(7):1434–1443. doi:10.1200/jco.22.00620
4. Fucikova J, Kepp O, Kasikova L, et al. Detection of immunogenic cell death and its relevance for cancer therapy. *Cell Death Dis*. 2020;11(11):1013. doi:10.1038/s41419-020-03221-2
5. Garland KM, Sheehy TL, Wilson JT. Chemical and biomolecular strategies for STING pathway activation in cancer immunotherapy. *Chem Rev*. 2022;122(6):5977–6039. doi:10.1021/acs.chemrev.1c00750
6. Jin WJ, Zangl LM, Hyun M, et al. ATM inhibition augments type I interferon response and antitumor T-cell immunity when combined with radiation therapy in murine tumor models. *J Immunother Cancer*. 2023;11(9):e007474. doi:10.1136/jitc-2023-007474
7. Wang Y, Liu ZG, Yuan H, et al. The reciprocity between radiotherapy and cancer immunotherapy. *Clin Cancer Res*. 2019;25(6):1709–1717. doi:10.1158/1078-0432.Ccr-18-2581
8. Du SS, Chen GW, Yang P, et al. Radiation therapy promotes hepatocellular carcinoma immune cloaking via PD-L1 upregulation induced by cGAS-STING activation. *Int J Radiat Oncol Biol Phys*. 2022;112(5):1243–1255. doi:10.1016/j.ijrobp.2021.12.162
9. Xing JL, Stea B. Molecular mechanisms of sensitivity and resistance to radiotherapy. *Clin Exp Metastasis*. 2024;41(4):517–524. doi:10.1007/s10585-023-10260-4
10. Aggarwal V, Workman CJ, Vignali DAA. LAG-3 as the third checkpoint inhibitor. *Nat Immunol*. 2023;24(9):1415–1422. doi:10.1038/s41590-023-01569-z
11. Shen R, Postow MA, Adamow M, et al. LAG-3 expression on peripheral blood cells identifies patients with poorer outcomes after immune checkpoint blockade. *Sci Transl Med*. 2021;13(608). doi:10.1126/scitranslmed.abf5107
12. Li R, Qiu J, Zhang Z, et al. Prognostic significance of Lymphocyte-activation gene 3 (LAG3) in patients with solid tumors: a systematic review, meta-analysis and pan-cancer analysis. *Cancer Cell Int*. 2023;23(1):306. doi:10.1186/s12935-023-03157-5
13. Jiang Y, Han Q, Zhao H, Zhang J. The mechanisms of HBV-induced hepatocellular carcinoma. *J Hepatocell Carcinoma*. 2021;8:435–450. doi:10.2147/jhc.S307962
14. Zhou Y, Tao L, Qiu J, et al. Tumor biomarkers for diagnosis, prognosis and targeted therapy. *Signal Transduct Target Ther*. 2024;9(1):132. doi:10.1038/s41392-024-01823-2
15. Liu M, Wen Y. Point-of-care testing for early-stage liver cancer diagnosis and personalized medicine: biomarkers, current technologies and perspectives. *Heliyon*. 2024;10(19):e38444. doi:10.1016/j.heliyon.2024.e38444
16. Zafar S, Hafeez A, Shah H, et al. Emerging biomarkers for early cancer detection and diagnosis: challenges, innovations, and clinical perspectives. *Eur J Med Res*. 2025;30(1):760. doi:10.1186/s40001-025-03003-6
17. Govindu S, Gowda P, Muquith M, Espinoza M, Hsiehchen D. Primary and secondary pseudo-stability and progression after atezolizumab with and without bevacizumab. *J Immunother Cancer*. 2026;14(1). doi:10.1136/jitc-2025-013727
18. Watanabe Y, Ogawa M, Tamura Y, et al. A case of pseudoprogression in hepatocellular carcinoma treated with atezolizumab plus bevacizumab. *J Investig Med High Impact Case Rep*. 2021;9:23247096211058489. doi:10.1177/23247096211058489
19. Vadevoo SMP, Gurung S, Lee HS, et al. Peptides as multifunctional players in cancer therapy. *Exp Mol Med*. 2023;55(6):1099–1109. doi:10.1038/s12276-023-01016-x
20. Chen Q, Shang W, Zeng C, et al. Theranostic imaging of liver cancer using targeted optical/MRI dual-modal probes. *Oncotarget*. 2017;8(20):32741–32751. doi:10.18632/oncotarget.15642
21. Hwang SY, Danpanichkul P, Agopian V, et al. Hepatocellular carcinoma: updates on epidemiology, surveillance, diagnosis and treatment. *Clin Mol Hepatol*. 2025;31(Suppl):S228–s254. doi:10.3350/cmh.2024.0824
22. Vogel A, Meyer T, Sapisochin G, Salem R, Saborowski A. Hepatocellular carcinoma. *Lancet*. 2022;400(10360):1345–1362. doi:10.1016/S0140-6736(22)01200-4
23. Di Y, Ren G, Wang Y, Meng L, Li J. Stereotactic body radiation therapy for hepatocellular carcinoma: a comprehensive review. *Front Oncol*. 2026;16:1747449. doi:10.3389/fonc.2026.1747449

24. Seyhan D, Allaire M, Fu Y, et al. Immune microenvironment in hepatocellular carcinoma: from pathogenesis to immunotherapy. *Cell Mol Immunol*. 2025;22(10):1132–1158. doi:10.1038/s41423-025-01308-4
25. Li M, Li T, Wu F, Ren F, Xue S, Li C. Advanced NIR-II fluorescence imaging technology for precise evaluation of nanomedicine delivery in cancer therapy. *Chemosensors*. 2024;12(6). doi:10.3390/chemosensors12060113
26. Que Y, Fang Z, Guan Y, et al. LAG-3 expression on tumor-infiltrating T cells in soft tissue sarcoma correlates with poor survival. *Cancer Biol Med*. 2019;16(2):331–340. doi:10.20892/j.issn.2095-3941.2018.0306
27. Goldberg MV, Drake CG. LAG-3 in Cancer Immunotherapy. *Curr Top Microbiol Immunol*. 2011;344:269–278. doi:10.1007/82_2010_114
28. Quan Z, Gao Y, Sun B, et al. Combination immunotherapy targeting LAG-3, PD-1 and STING suppresses hepatocellular carcinoma as monitored by LAG-3 targeted PET imaging. *Biomark Res*. 2025;13(1):102. doi:10.1186/s40364-025-00820-z
29. Liu J, Cheng P, Xu C, Pu K. Molecular probes for in vivo optical imaging of immune cells. *Nat Biomed Eng*. 2025;9(5):618–637. doi:10.1038/s41551-024-01275-7
30. Chen L, Lyu Y, Zhang X, et al. Molecular imaging: design mechanism and bioapplications. *Sci China Chemist*. 2023;66(5):1336–1383. doi:10.1007/s11426-022-1461-3
31. Cai M-Z, Wen Z, Li H-Z, et al. Peptide-based fluorescent probes for the diagnosis of tumor and image-guided surgery. *Biosens Bioelectron*. 2025;276:117255. doi:10.1016/j.bios.2025.117255
32. Guo Q, Liu A, Huang Y, et al. Small-molecule fluorescent probes for imaging and diagnosing ischemia-reperfusion injury. *Chin Chem Lett*. 2025;36(12):110943. doi:10.1016/j.cclet.2025.110943
33. Jiao Y, Cao F, Liu H. Radiation-induced cell death and its mechanisms. *Health Phys*. 2022;123(5):376–386. doi:10.1097/hp.0000000000001601
34. Liu S, Wang W, Hu S, et al. Radiotherapy remodels the tumor microenvironment for enhancing immunotherapeutic sensitivity. *Cell Death Dis*. 2023;14(10). doi:10.1038/s41419-023-06211-2
35. Gao L, Zhang A. Low-dose radiotherapy effects the progression of anti-tumor response. *Transl Oncol*. 2023;35:101710. doi:10.1016/j.tranon.2023.101710
36. Guo S, Yao Y, Tang Y, et al. Radiation-induced tumor immune microenvironments and potential targets for combination therapy. *Signal Transduct Target Ther*. 2023;8(1):205. doi:10.1038/s41392-023-01462-z
37. Wei X, Jiang Y, Li Y, et al. Enhanced efficacy and long-term survival with SBRT plus PD-1 inhibitors versus SBRT alone in unresectable HCC: a multicenter PSM study. *Oncologist*. 2026;31(3). doi:10.1093/oncolo/oyaf437
38. Li Z, Liu J, Zhang B, et al. Neoadjuvant tislelizumab plus stereotactic body radiotherapy and adjuvant tislelizumab in early-stage resectable hepatocellular carcinoma: the Notable-HCC phase 1b trial. *Nat Commun*. 2024;15(1):3260. doi:10.1038/s41467-024-47420-3

Journal of Hepatocellular Carcinoma

Dovepress
Taylor & Francis Group

Publish your work in this journal

The Journal of Hepatocellular Carcinoma is an international, peer-reviewed, open access journal that offers a platform for the dissemination and study of clinical, translational and basic research findings in this rapidly developing field. Development in areas including, but not limited to, epidemiology, vaccination, hepatitis therapy, pathology and molecular tumor classification and prognostication are all considered for publication. The manuscript management system is completely online and includes a very quick and fair peer-review system, which is all easy to use. Visit http://www.dovepress.com/testimonials.php to read real quotes from published authors.

Submit your manuscript here: https://www.dovepress.com/journal-of-hepatocellular-carcinoma-journal